Journal of
Composites Science

MDPI

Article

Towards 3D Pore Structure of Porous Gypsum Cement Pozzolan Ternary Binder by Micro-Computed Tomography

Girts Bumanis [1,*], Laura Vitola [1], Xiangming Zhou [2], Danutė Vaičiukynienė [3] and Diana Bajare [1]

[1] Institute of Sustainable Building Materials and Engineering Systems, Faculty of Civil and Mechanical Engineering, Riga Technical University, Kipsalas Str. 6A, LV-1048 Riga, Latvia; laura.vitola_1@rtu.lv (L.V.); diana.bajare@rtu.lv (D.B.)
[2] Department of Civil & Environmental Engineering, Brunel University London, Uxbridge UB8 3PH, UK; xiangming.zhou@brunel.ac.uk
[3] Faculty of Civil Engineering and Architecture, Kaunas University of Technology, Studentu St. 48, LT-51367 Kaunas, Lithuania; danute.vaiciukyniene@ktu.lt
* Correspondence: girts.bumanis@rtu.lv

Abstract: A sophisticated characterisation of a porous material structure has been challenging in material science. Three-dimensional (3D) structure analysis allows the evaluation of a material's homogeneity, pore size distribution and pore wall properties. Micro-computed tomography (micro-CT) offers a non-destructive test method for material evaluation. This paper characterises a novel ternary binder's porous structure using micro-CT. Gypsum–cement–pozzolan (GCP) ternary binders are low-carbon footprint binders. Both natural and industrial gypsum were evaluated as a major components of GCP binders. Porous GCP binder was obtained by a foaming admixture, and the bulk density of the material characterised ranged from 387 to 700 kg/m^3. Micro-CT results indicate that pores in the range from 0.017 to 3.0 mm can be effectively detected and described for porous GCP binders. The GCP binder structure proved to be dominant by 0.1 to 0.2 mm micropores. For GCP binders produced with natural gypsum, macropores from 2.2 to 2.9 mm are formed, while GCP binders with phosphogypsum possess pores from 0.2 to 0.6 mm. Micro-CT proved to be an effective instrument for characterising the homogeneity and hierarchical pore structure of porous ternary binders.

Keywords: ternary binder; phosphogypsum; lightweight; porous material; tomography

Citation: Bumanis, G.; Vitola, L.; Zhou, X.; Vaičiukynienė, D.; Bajare, D. Towards 3D Pore Structure of Porous Gypsum Cement Pozzolan Ternary Binder by Micro-Computed Tomography. *J. Compos. Sci.* **2024**, *8*, 264. https://doi.org/10.3390/jcs8070264

Academic Editor: Stelios K. Georgantzinos

Received: 21 May 2024
Revised: 17 June 2024
Accepted: 1 July 2024
Published: 8 July 2024

1. Introduction

Micro-computer tomography (micro-CT) plays a crucial role in advancing construction material research by providing detailed insights into the internal structure and properties of various materials. The visualisation of the internal microstructure of construction materials in three dimensions with high resolution is possible with the help of micro-CT. The examination of porosity through micro-CT for porous building materials (e.g., autoclaved aerated concrete) demonstrates the distribution of both open and closed pores within the modified material [1]. Micro-CT facilitates the quantification of porosity, pore size distribution, and pore connectivity within construction materials. This information is essential for understanding material properties, such as permeability, strength, and durability.

Micro-CT has been used extensively to characterise damage progression in materials. Micro-CT helps to track the initiation and propagation of cracks and defects within construction materials under various loading conditions. This aids in the evaluation of material performance and helps in developing strategies for improving fracture resistance and durability. Steel corrosion in concrete, concrete damage after freeze–thaw cycles, and fibre-reinforced composite damage have been investigated in various research reports [2,3]. The quantitative information obtained from micro-CT has been analysed using deep learn-

ing models as well [4]. D'haen et al. used computer tomography scanning ex situ to evaluate the evolution of damage for carbon fibre laminates [5].

There are certain limitations to micro-CT applications. The constraint is associated with the voxel resolution, and microscopic particles remaining unseen in the images. Depending on the device used, pore structures from 10 to 120 μm can be characterised effectively [6,7]. Utilising high-resolution micro-CT and advanced image processing technology, a three-dimensional (3D) pore structure model featuring macropores can be constructed, and the dimension of the representative elementary volume can be established. The description of pervious concrete through micro-CT indicated that approximately 80% of macropores fall within the range of 0.15–1 mm, while the spatial distribution of macropores revealed significant heterogeneity, leading to a permeability anisotropy index significantly exceeding 1, reaching up to 8 in some instances [8].

To produce high-performance construction materials, high porosity may lead to improved thermal conductivity and low density. Gypsum and cement can be used to produce porous materials [9–12]. Characterising porous structure and its homogeneity is still a challenge to the research community. Gypsum is well known for its low environmental impact compared to other traditional cementitious materials [13]. Together with bio-based aggregates, excellent CO_2 negative insulation materials can be produced both from natural gypsum and industrial by-products of gypsum, such as phosphogypsum (PG) [14,15]. However, gypsum's water resistance is low, which limits its wider applications [16]. In cement composites, it is established that the sulphur-related compounds (e.g., from wastewater) are responsible for the formation of gypsum as a secondary phase during the hydration of cement. This causes deleterious reactions and leads to severe damage and cracking of the cement-based materials [17]. The negative role that gypsum plays in cement-based materials has been widely investigated [18]. However, in ternary binders, gypsum and cement can be effectively used with the help of pozzolanic materials. Various research articles have reported the high performance of such binding materials, which also allows for using various by-products in the compositions [19–22]. PG has gained top priority in the research community, as its current application in the production of building materials is limited because of the safety concerns related to the impurities in the material [23,24]. In ternary binders, the potential hazards of the PG can be significantly reduced.

In this research, for the first time, porous ternary binders based on gypsum-cement-pozzolans (GCPs) are investigated with micro-CT. The effects of natural gypsum and PG on the pore structure formation are evaluated, and different microporous structures of GCP are obtained.

2. Materials and Methods

The main component of a GCP binder is gypsum. In this research, two types of gypsum were used. The first one, i.e., the phosphogypsum (PG) dihydrate sourced from Lifosa AB in Lithuania, was dried at 60 °C and milled with collision milling in a disintegrator to a particle size with a d_{50} of 74 μm [23]. Following this, the calcium sulphate hemihydrate binder was produced by heating PG dihydrate powders at 180 °C for 4 h. The chemical composition was detected with a wavelength-dispersive X-ray fluorescence analyser (ARL PERFORM'X, Thermo Fisher Scientific Inc., Denver, CO, USA). The loss on ignition (LOI) of the materials was determined by the EN 196-2. PG dihydrate powders consisted of 1.07% SiO_2, 0.70% Al_2O_3, 0.22% Fe_2O_3, 37.16% CaO, 0.21% MgO, 37.38% SO_3, 0.48% Na_2O, 0.11% TiO_2, and 0.57% P_2O_5, all by weight, and their loss on ignition was 19.24%.

For comparison, the other type of gypsum, from Knauf commercial gypsum plaster, was used. Its particle size was characterised by a coarser nature than that of PG dihydrates with a d_{50} of 140 μm. The chemical compositions of commercial gypsum plaster consisted of 3.73% SiO_2, 1.68% Al_2O_3, 0.46% Fe_2O_3, 35.64% CaO, 3.92% MgO, 30.90% SO_3, 0.31% Na_2O, and 0.05% TiO_2, again all by weight, and their loss on ignition was 22.43%.

Portland cement CEM I 42.5 N was used in the GCP composition. According to the Portland cement datasheets, its initial setting time according to EN 196-3 was 182 min,

while its final setting time was 224 min. Its normal consistency was 28.2%, while its Blaine fineness was 3787 cm^2/g. Additionally, its compressive strength reached 15.4, 32.9, 48.8 and 60.5 MPa, respectively, at 1, 2, 7 and 28 days.

Metakaolin-based by-products from foam glass production were acquired as pozzolanic material in the ternary binders to bind hazardous hydration products to avoid deleterious sulphate reaction. The physical and chemical properties of the metakaolin have been reported in previous papers [25]. The polycarboxylate superplasticiser and the setting retarder were used as chemical admixtures to produce a GCP slurry with a low water-to-solid binder ratio. Synthetic foaming agent (FS) Pb-Lux (Stroymechanika, Ltd., Tula, Russia) in the form of a 5% solution was used to prepare porous GCP material. SDS stabiliser (Sigma-Aldrich, Ltd., St. Louis, MO, USA) was incorporated into the material to stabilise the pore structure until the initial setting of the GCP binder.

The porous GCP mixture's compositions evaluated in this research are given in Table 1. The compositions of the GCP solid binder which is subjected to further foaming consist of gypsum–cement-pozzolan with a ratio of 1:0.4:0.4. The water-to-solid binder ratio was 0.3. Additionally, superplasticiser was added at the dosage of 1.5% by weight of solid binder as well as setting the retarder at the dosage of 0.2% by weight and stabiliser at 0.2% also by weight of the solid binder. To prepare the porous material, a foaming agent was used. In the case of G1 and P1, it was added at a dosage of 12% by weight of GCP, while in the case of G2 and P2, it was 8% by weight. After foam preparation, the slurry of GCP was incorporated into the foams and mixed thoroughly. Different porous structures of GPC have been formed because of the lower foam concentration in the mixture and the specific nature of the gypsum source.

Table 1. Mixture compositions of produced porous GCP material, kg/m^3.

		Composition			
		G1	**G2**	**P1**	**P2**
Components of solid binder, kg/m^3	Phosphogypsum dihydrate	-	-	313	345
	Commercial gypsum plaster	219	282	-	-
	CEM I	92	118	131	144
	Metakaolin	92	118	131	144
	Water, kg/m^3	108	139	170	183
	Water/solid of binder	0.3			
	Superplasticiser/solid binder	0.015		0.014	
	Set retarder/solid binder	0.002			
	Stabiliser/solid binder	0.002			
	Foaming agent/binder	0.12	0.08	0.12	0.08
	Total, kg/m^3	578	721	840	894
	Dry components, kg/m^3	404	519	576	633

A Le Chatelier flask was used to determine the density of the mixture and to calculate its total porosity. Apparent (open) porosity was measured by the water absorption principle according to ASTM C20-00. A LaserComp Fox600 (TA Instruments, New Castle, DE, USA) was used to determine the thermal conductivity for $35 \times 35 \times 5$ cm^3 foam GCP plates. The mechanical properties were determined using $5 \times 5 \times 5$ cm^3 cubical specimens with a Zwick Z100 testing machine (ZwickRoell, Ulm, Germany) (with a loading speed of 0.5 mm/min). The mico-CT 50 Scanco Medical AG, Wangen, Switzerland was used to characterise the pore structure of the GCP binders.

3. Results

3.1. Macrostructure of Porous GCP Binder

The macrostructure of the produced GCP binders is presented in Figure 1. Two different structures of the GCP binders at the macrostructure level have been obtained depending on the type of gypsum (i.e., PG or commercial gypsum plaster) used in the

composition (see Table 1). The G1 (see Figure 1a) and G2 (see Figure 1b) synthesised using commercial gypsum plaster present a large pore structure with pores up to 2 mm. A thin-walled structure with interconnected internal pores, as well as smaller pores between the walls of the larger pores, is clearly visible. Specifically, G1 shows larger pores (see Figure 1a) compared to G2 (see Figure 1b) because of differences in the concentration of the blowing agent in the mixtures.

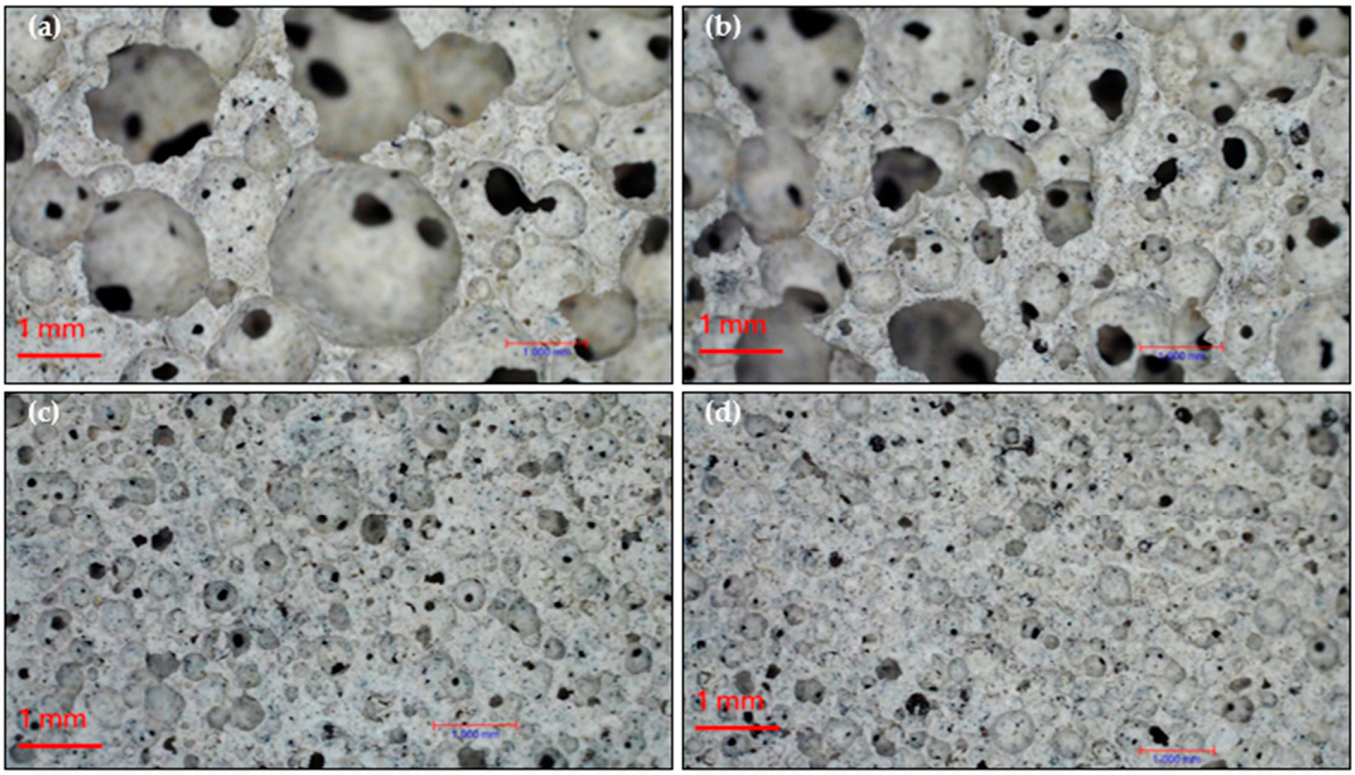

Figure 1. Macrostructure of the porous GCP material at 40× magnification. (**a**) G1; (**b**) P1; (**c**) G2; (**d**) P2.

The porous GCP binder containing PG (P1 and P2, respectively) has mainly smaller pores in its structure (Figure 1c,d). The macrostructure of P1 and P2 is more homogenous compared with G1 and G2. Both interconnected and closed pores with a pore size of up to 0.5 mm can be observed in the material. In addition, small fused pores can be observed in the structure of the foam material.

3.2. Physical Properties and Compressive Strength

Table 2 presents the summary of various physical and mechanical properties. The G1 and G2 samples have significantly lower density compared to P1 and P2. G1 has the lowest density of 387 ± 22 kg/m^3 compared to 523 ± 15 kg/m^3 of G2, while the porous GCP binders produced using PG exhibit a bulk density of 622 ± 12 kg/m^3 (P1) and 700 ± 11 kg/m^3 (P2). The total porosity of the porous GCP binder strongly affects the compressive strength. P1 and P2 with a total porosity of 72.0 ± 1.2 vol.% and 69.5 ± 1.2 vol.% have a compressive strength of 2.4 ± 0.25 and 5.4 ± 0.40 MPa, respectively. Meanwhile, porous GCP binders produced using commercial gypsum plaster demonstrate a compressive strength of 0.3 ± 0.05 MPa (G1) and 1.0 ± 0.03 MPa (G2) with the total porosity of 84 ± 2.0 vol.% and 78.5 ± 1.5 vol.%, respectively.

Table 2. Physical properties and compressive strength of porous GCP binders.

Composition	Bulk Density, kg/m^3	Total Porosity, vol.%	Thermal Conductivity, W/m·K	Compressive Strength, MPa
G1	387 ± 22	84.0 ± 2.0	0.086	0.3 ± 0.05
G2	523 ± 15	78.5 ± 1.5	0.123	1.0 ± 0.03
P1	622 ± 12	72.0 ± 1.2	0.111	2.4 ± 0.25
P2	700 ± 11	69.5 ± 1.2	0.153	5.4 ± 0.40

As the total porosity is one of the most important factors that affect the bulk density of the material, therefore it has an impact on the thermal conductivity as well. In accordance with the results presented in Table 2, relatively high thermal conductivity is presented for P1 and P2 (i.e., reaching 0.111 and 0.153 W/m·K, respectively), but G1 and G2 have a comparatively lower thermal conductivity, i.e., 0.086 and 0.123 W/m·K.

3.3. Structure Assessment of Porous GCP Binders

The reconstruction of the pore structure of porous GCP binders is given in Figure 2, in which, for porous GCP binder G1, the coalescence of larger pores can be observed. The higher amount of foaming agent in the mixture means that the pore system cannot be separated by the individual pores of the GCP matrix. Individual pores are visible in G2 (see Figure 2b), while the more even pore structure results in increased density and compressive strength. No visible difference can be identified in the case of the pore structure reconstruction of P1 (see Figure 1c) and P2 (see Figure 1d). The fine nature of the PG component in the GCP matrix allows the creation of a fine GCP binder matrix around the pores.

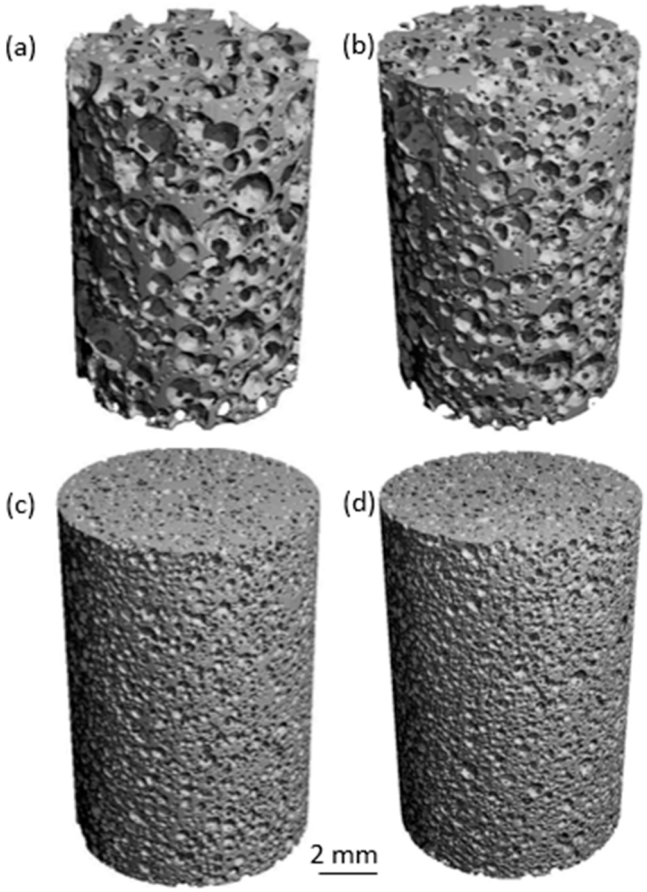

Figure 2. Reconstruction of pore structure of the GCP binder samples: (**a**) GCP binder mixture composition G1; (**b**) G2; (**c**) P1; (**d**) P2.

Under the segmented 3D model of the GCP binder pore structure (see Figure 3), the larger pores identified in G1 (see Figure 3a) demonstrate pore size distribution in a wide region. The G2 (see Figure 3b) has a more homogenous meso–macro-pore structure than G1. This correlates well with the bulk density and compressive strength (see Table 2).

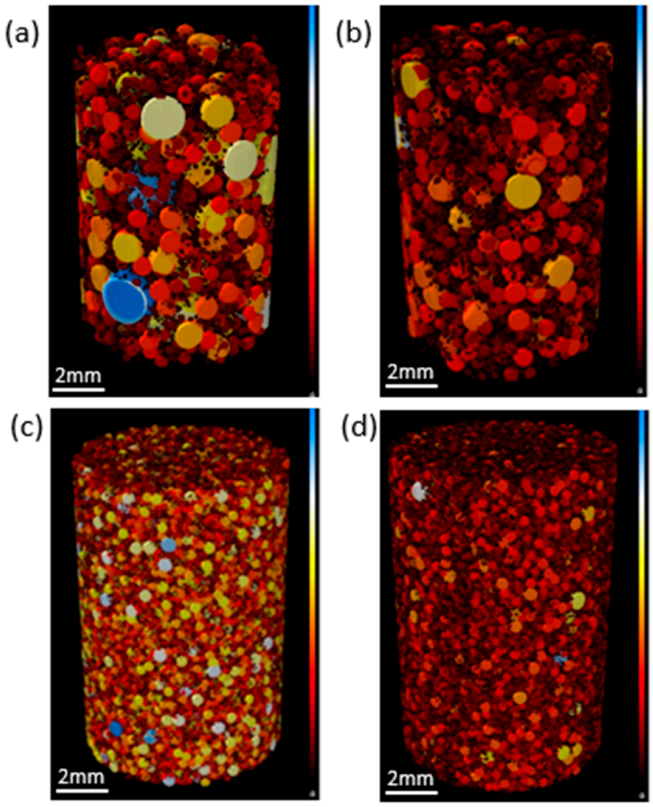

Figure 3. Three-dimensional (3D) model of segmented pore structure of the GCP binders: (**a**) G1; (**b**) G2; (**c**) P1; (**d**) P2.

The 2D slices of the porous GCP binders are shown in Figure 4. The contrast between the pores and material walls represents the pore distribution in the material. It must be noted that the cross-sections of the pores on the 2D slices do not represent the actual cross-section of the pore, as it might be cut in different places of the wall. It is visible that G1 has a larger volume of bigger pores, while G2 has only some larger pores. Also, G2 presents a more even pore size distribution compared to G1. P1 and P2 have very similar pore size distribution on micro-CT 2D slices (see Figure 4c,d).

The results of the pore size distribution analysis given in Figure 5 show the difference between porous GCP made using commercial gypsum plaster (G1 and G2) and porous GCP made using PG (P1 and P2). In the case of G1 and G2, pores up to 2.9 mm are typical. A varied and evenly distributed pore size range is the characteristic of G1, while for G2, there is a gap in pore size between 1.7 and 2.2 mm and from 2.5 to 2.9 mm.

A relatively small number of pores are in a size region from 0.07 to 0.35 mm compared to the P1 and P2 mixtures, while the 8 vol.% of pores are 0.12 mm. In total, 83 vol.% of pores have been detected by the micro-CT for porous GCP binder G1, compared to 87 vol.% for G2, while for P1 and P2, they are 95.5 vol.% and 90 vol.%, respectively.

Table 3 provides the physical properties of GCP obtained from the micro-CT test. The material composition (see Table 1), especially the type of gypsum used, significantly affects the structure of porous GCP. The pore density of the porous GCP made using PG (i.e., P1 and P2) is 2.7–3.8 times higher than that of the porous GCP made using commercial gypsum plaster (i.e., G1 and G2). This is also compatible with the data in Figure 5 as well as the pore size results (see Table 3). The type of gypsum used significantly affects the porous

structure and pore spacing of the obtained porous GCP. G1 and G2 have a pore spacing of 1.28 mm and 0.9 mm, but in the case of P1 and P2, it is 4.5 and 3.2 times higher, respectively.

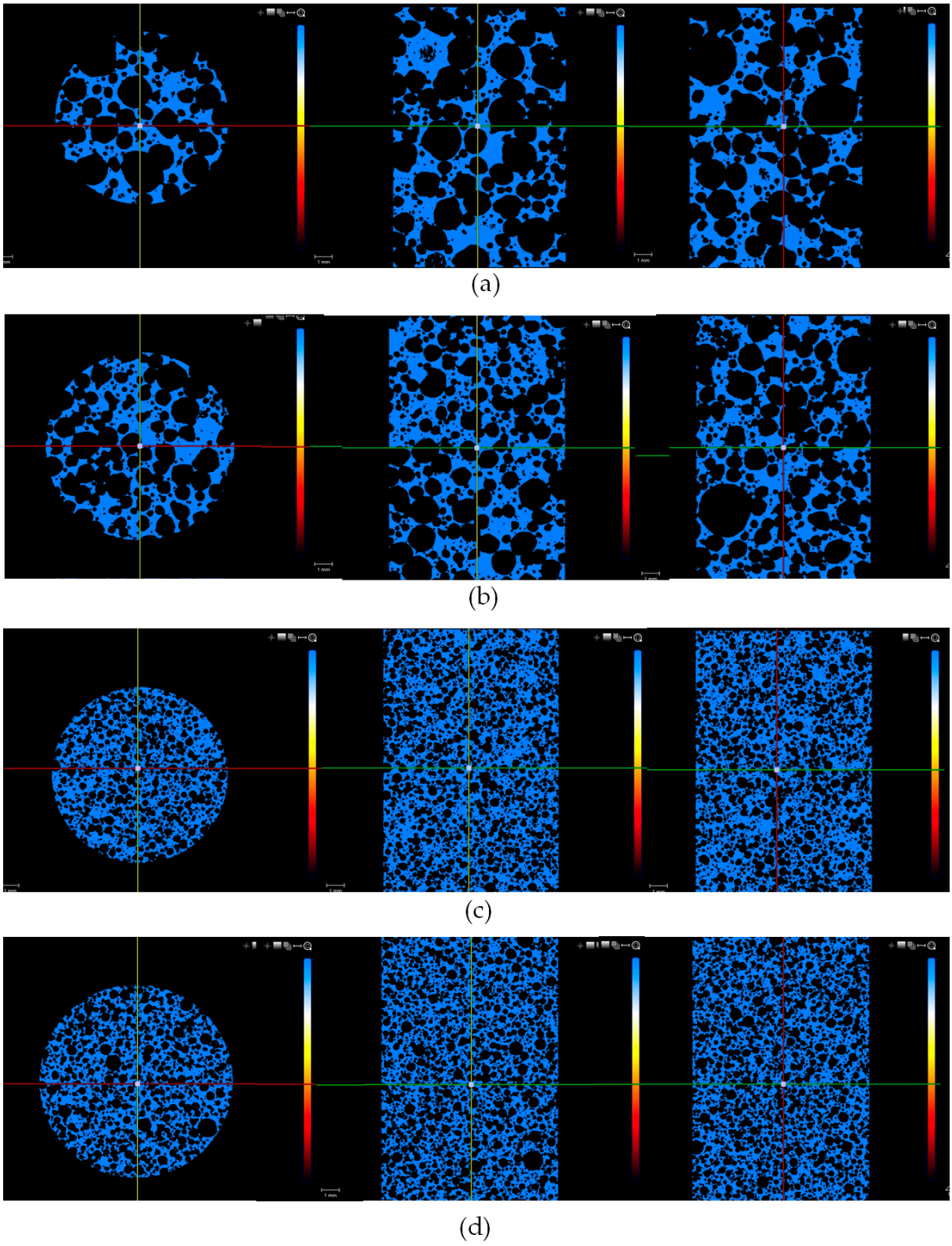

Figure 4. Cross-sections of porous GCP binders. (**a**) G1; (**b**) G2; (**c**) P1; (**d**) P2.

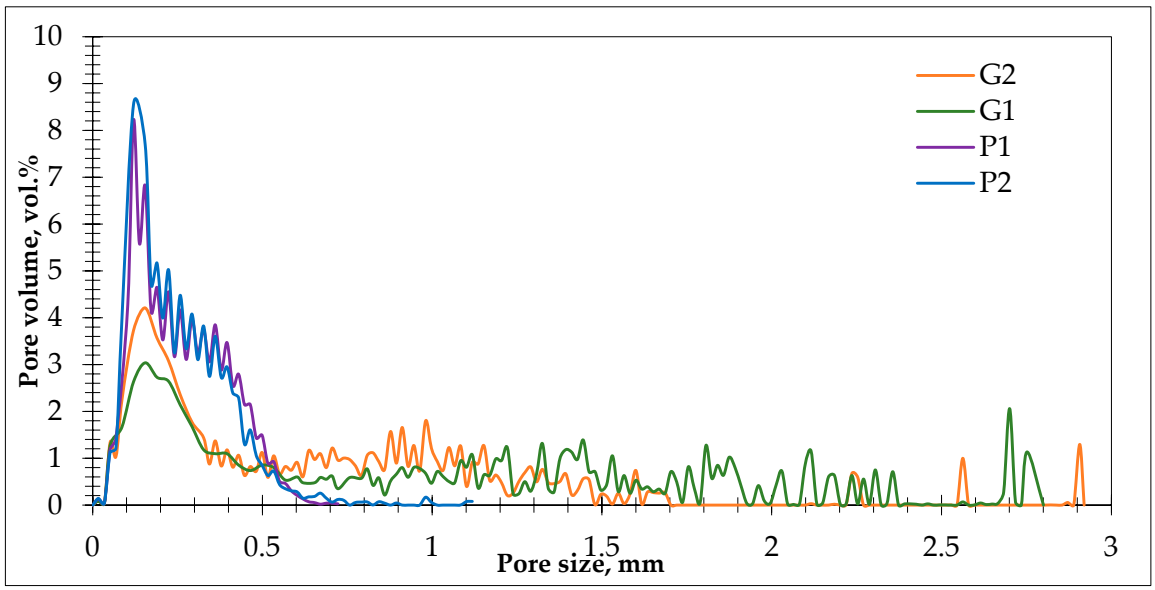

Figure 5. Pore size distribution of porous GCP.

Table 3. Physical properties of porous GCP binders in accordance with the micro-CT results.

	Composition			
	G1	**G2**	**P1**	**P2**
Pore density, mm	1.02	1.46	3.87	3.90
Pore size, mm^{-1}	0.27	0.23	0.13	0.12
Pore spacing, mm	1.28	0.90	0.28	0.28
Total porosity, %	68.40	63.30	48.14	51.95
Degree of anisotropy	1.04	1.02	1.00	1.02
Connectivity density, mm^{-3}	3.05	6.65	61.62	84.61

The total porosity analysed through micro-CT (see Table 3) demonstrates a reduction ranging from 15.2% to 23.9% compared to the experimentally obtained porosity (see Table 2). Samples based on commercial gypsum plaster (G1 and G2) exhibit a relatively smaller deviation with reductions of 15.6% for G1 and 15.2% for G2. Meanwhile, samples made of PG present higher reductions, i.e., 23.9% for P1 and 17.6% for P2, respectively.

As can be seen in Table 3, P1 has a homogenous pore structure with a high homogeneity degree of 1.00. The visual structure appearance in all directions supports this measurement (see Figure 4c), and the degree of anisotropy proves that the obtained porous GCP microstructure exhibits complete directional dependence, so the obtained material behaves differently along different orientations with no symmetry or uniformity in its properties across different directions. For other compositions, the degree of anisotropy is slightly higher, reaching 1.02 to 1.04 (see Table 3).

The micro-CT provides the results of connectivity density and, as presented in Table 3, the type of gypsum used significantly affected it. The porous GCP made using commercial gypsum plaster (G1 and G2) presents a connectivity density of 3.05 mm^{-3} and 6.65 mm^{-3}, respectively. P1 and P2 (porous GCP made using PG) have 20.2 and 12.7 times higher connectivity density, respectively.

4. Discussion

By changing the foaming agent concentration (8% or 12% by weight of fresh GCP binder) and water used in the preparation of foamed GCP binders, highly porous material with different bulk densities can be obtained. The use of different gypsum sources with the changing fineness of the binders results in a completely different macrostructure of the GCP. Commercial gypsum gives a large macropore structure with a pore size of up to

3 mm, while a finer PG binder results in a homogenous and fine pore structure. With the decrease in pore size, the bulk density of GCP increases from 387 to 700 kg/m^3, and the compressive strength improves from 0.3 to 5.4 MPa. The amount of foaming agent added also plays a role in the porous structure.

Micro-CT allows inspecting the foamed GCP material without destruction of the structure and allows the complete characterisation of the pore and pore wall structure. The limitation observed by micro-CT is associated with micropores with a size below 50 µm, which cannot be detected by the machine used in this research. This is the reason why the total porosity differs between experimental results and results obtained from micro-CT. The 15 to 23 vol.% of total pore volume can be attributed to the pores below 50 µm.

Micro-CT allows to characterise pore density in the GCP binders. Pore density refers to the number of pores present within a given volume of the imaged sample, and a good correlation with pore size can be achieved. Larger pores for GCP with commercial gypsum have a pore density from 1.02 to 1.46 mm, while GCP made with PG has more pores in the volume of the material, reaching 3.87 to 3.90 mm. The pore size obtained by micro-CT determines the size distribution of pores within a sample based on the three-dimensional imaging data. Pore spacing characterises the distance between individual pores within a GCP binder. A lower pore spacing is for GCP made with PG, and it increases with the pore size for GCP made with commercial gypsum.

A very homogeneous pore structure was obtained for all mixtures, which is supported by the micro-CT results. The degree of anisotropy indicated that properties in different directions are similar, as the degree of anisotropy is in the range from 1.00 to 1.04. This can be achieved by the stabilising agent SDS used in the preparation of the foamed GCP as well as a low water-to-binder ratio, which is achieved by the use of a superplasticiser.

Connectivity density describes the interconnected pore network of the GCP binder, which can have implications for properties such as permeability, mechanical strength, and the transport of fluids or particles within the material [26]. Lower connectivity density was detected for GCP made with PG, which means the pores are relatively isolated or disconnected from each other, while the higher connectivity density for GCP made with commercial gypsum gives a greater degree of interconnectivity between the pores and, therefore, highly permeable material can be obtained.

The pore structure of the evaluated GCP material, including the size, distribution, and connectivity of its pores, significantly impacts its end-use properties. Smaller and more uniformly distributed pores, such as those in the P1 and P2 mixture compositions, enhance mechanical strength by relieving stress within the material and reducing the likelihood of crack initiation and propagation. High pore connectivity increases permeability, which is crucial for applications in civil engineering, and porous GCP made of commercial gypsum gives large pores with high permeability. A well-optimized pore structure could improve durability by making the material more resistant to environmental factors such as freeze–thaw cycles, chemical attacks, and water ingress. The void volume balances weight and strength, reducing the material's density without compromising the structural integrity.

5. Conclusions

The ternary binders containing gypsum as a major part of the binder, together with Portland cement and pozzolan, can be used to produce highly porous material. By changing the pore-forming admixture content and water consumption in foam preparation, materials with different densities can be obtained. The selection of gypsum and its fineness can contribute to the physical and mechanical properties significantly. However, to completely describe the pore structure of high-pore volume materials, micro-tomography (micro-CT) can be effectively used. Micro-CT has limitations when analysing microscale pores, as it can give different total pore volume results that are different from the experimentally obtained values, but the pore homogeneity, pore volume and parameters that describe the interconnectivity of the pores can be effectively measured. Understanding and optimising

pore structure is essential for tailoring materials to meet specific performance and durability requirements in various applications.

Author Contributions: Conceptualisation, G.B., D.V. and D.B.; methodology, G.B., D.V. and D.B.; software, L.V. and X.Z.; validation, X.Z., D.V. and D.B.; formal analysis, G.B. and L.V.; investigation, G.B. and L.V.; resources, D.B.; data curation, G.B. and L.V.; writing—original draft preparation, G.B. and L.V.; writing—review and editing, X.Z. and D.V.; visualisation, G.B. and L.V.; supervision, X.Z. and D.B.; project administration, D.B.; funding acquisition, D.B. All authors have read and agreed to the published version of the manuscript.

Funding: This research is funded by the FLPP (Fundamental and Applied Research Projects) Program in Latvia under the research project lzp-2022/1-0585 "Development and characterization of sustainable gypsum-cement-pozzolanic ternary compositions for 3D printing".

Data Availability Statement: The original contributions presented in the study are included in the article, further inquiries can be directed to the corresponding author.

Conflicts of Interest: The authors declare no conflicts of interest.

References

1. Stepien, A.; Dachowski, R. The Use of the Computer Tomography Method in the Analysis of the Microstructure of Materials Formed as a Result of Hydrothermal Treatment: Cellular Concretes. *J. Compos. Sci.* **2024**, *8*, 98. [CrossRef]
2. Zhang, M.; Wang, W. Deep Learning-Based Extraction and Quantification of Features in XCT Images of Steel Corrosion in Concrete. *Case Stud. Constr. Mater.* **2024**, *20*, e02717. [CrossRef]
3. Xin, C.; Yang, Y.; Yang, M.; Di, J.; Sun, Y.; Liang, P.; Wang, Y. Multi-Scale Analysis of the Damage Evolution of Coal Gangue Coarse Aggregate Concrete after Freeze–Thaw Cycle Based on CT Technology. *Materials* **2024**, *17*, 975. [CrossRef] [PubMed]
4. Badran, A.; Parkinson, D.; Ushizima, D.; Marshall, D.; Maillet, E. Validation of Deep Learning Segmentation of CT Images of Fiber-Reinforced Composites. *J. Compos. Sci.* **2022**, *6*, 60. [CrossRef]
5. D'haen, J.J.A.; May, M.; Boegle, C.; Hiermaier, S. Damage Evolution Analysis on Compression-Loaded Multidirectional Carbon Fiber Laminates Using Ex-Situ CT Scans. *J. Compos. Sci.* **2022**, *6*, 63. [CrossRef]
6. Xie, X.; Liu, X.; Zhang, L. New Insight on Particle Migration of Concrete under Pumping Based on X-ray Computed Tomography. *Cem. Concr. Compos.* **2024**, *149*, 105492. [CrossRef]
7. Reedy, C.L.; Reedy, C.L. High-Resolution Micro-CT with 3D Image Analysis for Porosity Characterization of Historic Bricks. *Herit. Sci.* **2022**, *10*, 83. [CrossRef]
8. Cai, P.; Mao, X.; He, P.; Lai, X. Quantifying Three-Dimensional Macropore Structure and Seepage Characteristics of Representative Elementary Volume for Recycled Aggregate Pervious Concrete. *J. Mater. Civ. Eng.* **2024**, *36*, 04024092. [CrossRef]
9. Roch, E.; Messing, G.L. Direct Foaming and Seeding of Highly Porous, Lightweight Gypsum. *J. Mater. Res.* **2016**, *31*, 2244–2251. [CrossRef]
10. Sahmenko, G.; Korjakins, A.; Namsone, E. High Performance Foam Concrete Produced in Turbulence Mixers. In Proceedings of the SBE 16 Malta Europe and the Mediterranean towards a Sustainable Built Environment, Valletta, Malta, 16–18 March 2016; pp. 71–78.
11. Doleželová, M.; Krejsová, J.; Vimmrová, A. Lightweight Gypsum Based Materials: Methods of Preparation and Utilization. *Int. J. Sustain. Dev. Plan.* **2017**, *12*, 326–335. [CrossRef]
12. Vimmrová, A.; Keppert, M.; Svoboda, L.; Černý, R. Lightweight Gypsum Composites: Design Strategies for Multi-Functionality. *Cem. Concr. Compos.* **2011**, *33*, 84–89. [CrossRef]
13. Bumanis, G.; Vitola, L.; Pundiene, I.; Sinka, M.; Bajare, D. Gypsum, Geopolymers, and Starch-Alternative Binders for Bio-Based Building Materials: A Review and Life-Cycle Assessment. *Sustainability* **2020**, *12*, 5666. [CrossRef]
14. Bumanis, G.; Irbe, I.; Sinka, M.; Bajare, D. Biodeterioration of Sustainable Hemp Shive Biocomposite Based on Gypsum and Phosphogypsum. *J. Nat. Fibers* **2021**, *19*, 10550–10563. [CrossRef]
15. Chakarala, V.; Schuster, J.; Shaik, Y.P. Development and Characterization of Flax–Gypsum Composites. *J. Compos. Sci.* **2024**, *8*, 27. [CrossRef]
16. Shanbayev, M.; Turgumbayeva, K.; Blumberga, D.; Aipenova, A.; Beisekova, T. Environmental and Economic Advantages of Disposal of Phosphoric Industry Waste. *Environ. Clim. Technol.* **2022**, *26*, 143–154. [CrossRef]
17. Kashaija, N.T.; Gável, V.; Gergely, K.; Akos, K.; Kürthy, M.; Szabó, C.; Tóth, E.; Szabó-Krausz, Z. Deterioration of Cementitious Materials in Wastewater Treatment Plants' Pumping Stations and Sand-Trap Structures. *J. Compos. Sci.* **2024**, *8*, 60. [CrossRef]
18. Tian, B.; Cohen, M.D. Does Gypsum Formation during Sulfate Attack on Concrete Lead to Expansion? *Cem. Concr. Res.* **2000**, *30*, 117–123. [CrossRef]
19. Pan, H.; Wu, X.; Song, K.; Zhang, Y.; Zhao, Q. Preparation of Calcium Sulphoaluminate Cement-Portland Cement-Gypsum Based Sleeve Grouting Material: Performance Optimization and Tensile Properties of Sleeve Connector. *Constr. Build. Mater.* **2024**, *418*, 135341. [CrossRef]

20. Mármol, G.; Savastano, H.; Monzó, J.M.; Borrachero, M.V.; Soriano, L.; Payá, J. Portland Cement, Gypsum and Fly Ash Binder Systems Characterization for Lignocellulosic Fiber-Cement. *Constr. Build. Mater.* **2016**, *124*, 208–218. [CrossRef]
21. Tzouvalas, G.; Rantis, G.; Tsimas, S. Alternative Calcium-Sulfate-Bearing Materials as Cement Retarders: Part II. FGD Gypsum. *Cem. Concr. Res.* **2004**, *34*, 2119–2125. [CrossRef]
22. Taher, M.A.; Amine, A.M.; Damarany, B.K. Effect of Partial Substitution of Raw Gypsum with Thermally Treated Phosphogypsum on the Properties of Portland Pozzolanic Cement. *Adv. J. Chem. Sect. A* **2019**, *2*, 296–315. [CrossRef]
23. Bumanis, G.; Zorica, J.; Bajare, D. Properties of Foamed Lightweight High-Performance Phosphogypsum-Based Ternary System Binder. *Appl. Sci.* **2020**, *10*, 6222. [CrossRef]
24. Fornés, I.V.; Vaičiukynienė, D.; Nizevičienė, D.; Doroševas, V.; Michalik, B. A Comparative Assessment of the Suitability of Phosphogypsum from Different Origins to Be Utilised as the Binding Material of Construction Products. *J. Build. Eng.* **2021**, *44*, 102995. [CrossRef]
25. Bumanis, G.; Vitola, L.; Stipniece, L.; Locs, J.; Korjakins, A.; Bajare, D. Evaluation of Industrial By-Products as Pozzolans: A Road Map for Use in Concrete Production. *Case Stud. Constr. Mater.* **2020**, *13*, e00424. [CrossRef]
26. Klintström, E.; Smedby; Klintström, B.; Brismar, T.B.; Moreno, R. Trabecular Bone Histomorphometric Measurements and Contrast-to-Noise Ratio in CBCT. *Dentomaxillofacial Radiol.* **2014**, *43*, 20140196. [CrossRef]